FIXED PITCH ROTOR PERFORMANCE OF LARGE HORIZONTAL AXIS WIND TURBINES

Larry A. Viterna and Robert D. Corrigan
NASA Lewis Research Center
Cleveland, Ohio

ABSTRACT

Experimental fixed pitch wind turbine performance data is presented for both the DOE/NASA Mod-0 and the Danish Gedser wind turbines. Furthermore, a method for calculating the output power from large fixed pitch wind turbines is presented. Modifications to classical blade element-momentum theory are given that improve correlation with measured data. Improvement is particularly evident in high winds (low tip speed ratios) where aerodynamic stall occurs as the blade experiences high angles of attack.

INTRODUCTION

Recent tests on the NASA Mod-0 100kW wind turbine indicate that classical blade element-momentum theory is inadequate when the airfoils are at high angles of attack. This problem is particularly important in the calculation of fixed pitch and tip control rotor performance. Since the maximum power produced by a fixed pitch rotor is a critical design parameter, efforts are being made to improve theoretical analysis of this operating condition.

Experimental data from two Mod-0 rotor configurations as well as from the Danish Gedser wind turbine were analyzed. An empirical correction to the aerodynamic characteristics is presented which shows good agreement with the experimental results.

EXPERIMENTAL DATA

Tests were run on the NASA Mod-0 100 kW wind turbine to investigate the performance characteristics of fixed pitch rotors. Two rotors were used in the Mod-0 tests, both of which were 38 meters in diameter. Details of the blade planform, twist, etc. are given in Tables 1a and 1b and Figures 1a and 1b. Significant differences between the two blades are that the aluminum blades have a variable

thickness to chord ratio (t/c) and 34 degrees of non-linear twist, while the steel spar blades have a constant t/c and no twist. The thickness and twist distributions for the aluminum blades are given in Figures 2a and 2b.

The Mod-0 wind turbine was operated with the highly twisted aluminum blades at nominal rotor speeds of 20 and 26 rpm. Due to slip of the fluid coupling in the drive train, actual rotor speeds were 21.0 and 27.4 rpm at the maximum power of 50 kW and 105 kW respectively. Alternator output power and reference windspeed were recorded on magnetic tape and analyzed using the method of bins [ref. 1]. Figure 3 shows the median measured output power versus reference windspeed. The reference windspeed is measured by an anemometer located at hub height about 60 meters upwind of the rotor. This location is believed to give windspeeds which are representative of the average freestream windspeed at the rotor. The most interesting characteristic of the curves is the relatively constant output power at high windspeeds for both rotor speeds. The leveling off of the power output occurs for wind speeds at which stall occurs over most of the blade. Maximum power is greater for the higher rotor speed since higher wind speed is required to achieve the same stall angle of attack.

Further tests were conducted using the steel spar blades with no twist. The rotor speed was 32 rpm. The inboard 70 percent of the blade remains fixed in pitch and thus experiences high angles of attack at high windspeeds. As the wind speed increases, the wind turbine power output increases until the generator rating of 100 kW is reached. When wind speed increases further, it is necessary to pitch the outboard blade section so that the generator rating will not be exceeded. The tip pitch angle versus nacelle windspeed is given in Figure 4. The nacelle wind speed is measured by an anemometer located on the wind turbine nacelle. As shown in Figure 4, the outboard section pitching continues to increase as wind speed increases. This data indicates a continuing production of torque by the inboard fixed pitch portion, of the blade even though that section is stalled.

Finally, performance data from the fixed pitch Gedser wind turbine [ref. 2] is presented in Figure 5. Table 2 and Figure 6 present the rotor configuration for this wind turbine which operated in Denmark beginning in 1957. Though not much data was recorded for very high winds, operators of the Gedser turbine also reported constant power at windspeeds above stall.

Classical Theory

Blade element-momentum theory used in the PROP Code [ref. 3], as well as others, divides the blade into small spanwise elements. These elements are each considered to act as airfoil segments in two-dimensional flow fields, each at a particular angle of attack. From the geometry, the rotational velocity component, the wind

component, and the "induced" axial and rotational components, the local angle of attack is calculated. The lift and drag forces on the elements are then determined from two-dimensional (infinite aspect ratio) wind tunnel data at the local angle of attack [ref. 4]. Comparison of cambered and uncambered data indicates little difference in airfoil performance beyond stall. Therefore, data for symetric sections may be used [ref. 5, 6]. The "induced effects" of the wind turbine on the flow are determined in an iterative procedure until momentum theory is satisfied. The end effects of the finite length wind turbine blade are included by using a tip loss model. There are a variety of these tip loss models, the simplest being to reduce the lift coefficient to zero for approximately 3 percent of the radius near the tips. A more complete description of blade element-momentum theory, is contained in reference 3.

The Mod-0 aluminum blade rotor was modelled with the PROP Code. The aerodynamic data used is given in Figure 7 for a NACA 23018 "half-rough" airfoil. The designation "half-rough" denotes aerodynamic data which is an average of NACA smooth and rough data given in reference 4. This roughness effect was included to account for manufacturing imperfections and for the accumulation of dirt as the airfoil is exposed to the environment.

Since the output of the PROP Code is rotor power with no drive train losses, the following drive train efficiency model based on experimental data was used to calculate the electrical power:

(1) $$P_3 = -1.932 + 0.8238\ P_2$$

in which P_3 is the electrical power, (kW) and P_2 is the rotor power, (kW).

Figure 8 shows the predicted power versus windspeed for the Mod-0 aluminum blades using the PROP Code. The correlation between measured data and aralysis using infinite aspect ratio airfoil data is not very good. Similar results were obtained for the Mod-0 steel spar blade [Figure 9] and the Gedser wind turbine [Figures 10]. Smooth airfoil data was used for the Gedser wind turbine since standard rough data was not readily available for the its airfoil (Clark-Y). The most apparent deficiencies of the predicted results are (1) the rapid increase in power before stall, (2) the less-than-measured maximum power, and (3) the decrease in power after stall.

Improved Model

By manipulation of the airfoil characteristics the PROP Code was able to match the measured performance of the Mod-0 and Gedser wind turbines. A reduction in the unstalled lift curve slope, an increase

in the drag coefficient before stall, and a decrease in the drag coefficient after stall were required. It was observed that the resulting airfoil characteristics were approximately the same as those of a finite length wing with the same aspect ratio.

The formulas for converting infinite length airfoil data to finite length data are from the work of Munk, Glauert, and Prandtl. The equations are [ref. 7] given by the following:

$$(2a) \qquad C_L = C_{L_0}$$

$$(2b) \qquad C_D = C_{D_0} + \frac{C_L^2}{\pi AR}(1 + \sigma)$$

$$(2c) \qquad \alpha = \alpha_0 + \frac{57.3\ C_L}{\pi\ AR}\ (1 + \tau)$$

in which:

- C_L is the lift coefficient
- α is the angle of attack, deg
- C_D is the drag coefficient
- AR is the aspect ratio
- τ σ are factors to allow for the change from elliptical span loading to an airfoil with rectangular loading
- 0 is a subscript denoting infinite aspect ratio data

The actual aerodynamic load distribution on a wind turbine blade varies with windspeed, twist, planform, etc. However, since the factors τ and σ are small, the loading has been assumed elliptical (τ,σ are zero). The above corrections are made to the airfoil data below stall. Furthermore, because the end effects of the blade have been accounted for in the airfoil characteristics, the tip loss model has been eliminated.

It should be noted that the above corrections are empirical. The use of airfoil characteristics for infinite span in classical theory is regarded as established. The fact remains, however, that classical theory appears incapable of predicting performance at high angles of attack which occur for low aspect ratio blades at low rotor tip speed ratios. In the extreme, for example, at a tip speed ratio of zero (0 rpm) classical theory would predict the thrust on the rotor to be proportional to the drag coefficient of about 2 for an infinite aspect ratio [ref. 5]. We know, however, this is not true. The drag coefficient for even a flat plate of aspect ratio 8 is less than

1.3 [ref. 8]. It could be that assumption in momentum theory of an infinite number of lightly loaded blades needs to be reassessed and improved theoretical models developed for this condition.

Investigation of the airfoil characteristics after stall reveals the reason for the predicted negative power at very high winds. Figure 11 shows an airfoil element operating with its chord line parallel to the plane of rotation (as on the steel spar rotor). The resultant wind velocity acts at an angle of attack, α , with respect to the plane of rotation. The coefficients of lift, C_L, and drag, C_D, forces operating on the element can be resolved into a coefficient of torque force, C_Q , which acts in the plane of rotation. This coefficient is given by

$$C_Q = C_L \sin\alpha - C_D \cos\alpha \tag{3}$$

Using the infinite aspect ratio data from Figure 7 it can be seen in Figure 12 that negative torque can be expected for angles of attack between stall and 45 degrees.

The airfoil characteristics after stall were determined for an idealized stall which would result in constant power (torque) at high angles of attack. The torque force on a blade element is proportional to the coefficient of torque force and the square of the resultant velocity or mathematically

$$Q \sim C_Q V_R^2 \tag{4}$$

For a constant rotor speed we can divide by the constant V_Ω^2 which yields

$$Q \sim C_Q \frac{V_R^2}{V_\Omega^2} \tag{5}$$

but from Figure 11 $\cos\alpha = V_\Omega / V_R$ and thus

$$Q \sim \frac{C_Q}{\cos^2\alpha} \tag{6}$$

Substituting Eq. (3) gives

$$Q \sim \frac{C_L \sin\alpha}{\cos^2\alpha} - \frac{C_D}{\cos\alpha} \tag{7}$$

If we let

$$C_L = A_1 \sin 2\alpha + A_2 \frac{\cos^2\alpha}{\sin \alpha} \tag{8}$$

and

$$C_D = B_1 \sin^2\alpha + B_2 \cos \alpha \tag{9}$$

and substitute into Eq. (7) we have

$$Q \sim (2A_1 - B_1)\sin\alpha \tan \alpha + (A_2 - B_2) \tag{10}$$

Since the measured torque after stall is independent of wind speed it must also be independent of angle of attack. Thus, taking the derivative with respect to α and setting it equal to zero yields

$$A_1 = \frac{B_1}{2} \tag{11}$$

Referring to Figure 13, at an angle of attack of 90 degrees equation (9) gives

$$B_1 = C_{DMAX} \tag{12}$$

For a finite aspect ratio blade

$$C_{DMAX} \simeq 1.11 + 0.018 AR \tag{13}$$

for $AR \leq 50$ based and experimental data from Reference 8.

Thus

$$A_1 = \frac{C_{DMAX}}{2} \tag{14}$$

Rearranging Eq. (8) and substituting Eq. (14) yields

$$A_2 = (C_L - C_{DMAX} \sin \alpha \cos \alpha) \frac{\sin \alpha}{\cos^2\alpha} \tag{15}$$

Similarly Eqs. (9) and (12) give

$$B_2 = \frac{C_D - C_{DMAX} \sin^2\alpha}{\cos \alpha} \tag{16}$$

For continuity with the below stall airfoil data, A_2 and B_2 are solved at the stall angle condition and thus Eqs. (15) and (16) become

$$A_2 = (C_{L_s} - C_{DMAX} \sin \alpha_s \cos \alpha_s) \frac{\sin \alpha_s}{\cos^2 \alpha_s} \tag{17}$$

and

$$B_2 = C_{D_s} - \frac{C_{DMAX} \sin^2 \alpha_s}{\cos \alpha_s} \tag{18}$$

in which the subscript s denotes the value of the constant at stall.

The resulting airfoil characteristics for a NACA 23018 airfoil with an aspect ratio of 25 are given in Figure 14 and 15 along with the characteristics for an infinite aspect ratio airfoil [Fig. 8]. With these corrections to the airfoil characteristics, the predicted performance of the Mod-0 aluminum blade is found to correlate well with the measured data as shown in Figure 16. Similar results were obtained for the Mod-0 steel spar blade and the Gedser wind turbine are shown in Figures 17 and 18.

CONCLUSIONS

A method of correcting the airfoil characteristics for use with blade element-momentum theory has been developed. The airfoil data below stall is corrected for the finite length of the blade. This approach appears to account for the induced effects better than classical blade element-momentum theory alone, particularly for highly loaded low aspect ratio blades. An idealized model for aerodynamic characteristics after stall has been developed which results in nearly constant power in high winds. This model shows good agreement with experimental data from two rotor configurations on Mod-0 as well as the Danish Gedser wind turbine.

NOMENCLATURE

AR	aspect ratio of blade, R/c, based chord length at 75 percent radius
A_1, A_2	constants in lift coefficient equation after stall
B_1, B_2	constants in drag coefficient equation after stall
c	chord length, m
C_D	drag force coefficient
C_{Dmax}	drag force coefficient at 90° angle of attack
C_L	lift force coefficient
C_Q	torque force coefficient
P_2	rotor output power, kW
P_3	electrical output power, kW
Q	torque force, N
r	local radius, m
R	radius of rotor blade, m
V_R	resultant velocity vector, m/s
V_o	free-stream wind speed, m/s
V_1	wind velocity at rotor plane, m/s
V	velocity due to rotation, m/s
α	angle of attack, deg
τ σ	factors to allow for the change from elliptical span loading to an airfoil with rectangular loading
0	denotes infinite aspect ratio airfoil data
s	value of airfoil characteristic at stall

REFERENCES

1. Richards, T.R. and Neustadter, H.E.: DOE/NASA Mod-OA Wind Turbine Performance. DOE/NASA 1004-78/13 NASA TM-78916, 1978.

2. Interim Report on the Measurements on the Gedser Wind Mill, Per Lundsager, ed., Gedser Test Group, 1978.

3. Wilson, R.E. and Lissaman, P.B.S.: Applied Aerodynamics of Wind Power Machines. Oregon State University, July 1974. NSF/RA/N-74-113, PB-238595/3.

4. Abbott, I.H., Von Doenhoff, A.E. and Stivers, L.S.: Summary of Airfoil Data. NACA Report No. 824, 1945.

5. Critzos, C.C., Heyson, H.H. and Boswinkle, R.W.: Aerodynamic Characteristics of NACA 0012 Airfoil Section at Angles of Attack from 0° to 180°. NACA TN 3361, 1955.

6. Sheldehl, R.E., Klimas, P.C.: Aerodynamic Characteristics of Seven Symmetrical Airfoil Sections through 180-Degree Angle of Attack for Use in Aerodynamic Analysis of Vertical Axis Wind Turbines. SAND80-2114, 1981.

7. Jacobs, E.M. and Abbot, I.H., "The NACA Variable-Density Wind Tunnel," NACA TR 416, 1932.

8. Hoerner, S.F.: Fluid Dynamic Prog. Published by author, 1965.

TABLE 1a

ALUMINUM BLADE CHARACTERISTICS

Rotor dia., m(ft)	38.5 (126.4)
Number of Blades	2
Root cutout, % span	5
Fixed Pitch	--
Airfoil	NACA 230 Series
Taper	Linear
Twist, deg	34 (Non-linear)
Solidity	0.031
Precone, deg	0
Tilt, deg	8.5

TABLE 1b

STEEL SPAR BLADE CHARACTERISTICS

Rotor dia., m(ft)	38.4 (126.0)
Number of Blades	2
Root Cutout, % span	23
Tip Control, % span	30
Blade Pitch 75% span, deg	0
Airfoil	NACA 23024
Taper	Linear
Twist, deg	0.033
Precone, deg	0
Tilt, deg	8.5

TABLE 2

GEDSER BLADE CHARACTERISTICS

Rotor dia, m(ft)	24 (28.7)
Number of Blades	3
Root cutout, % span	25
Fixed Pitch	--
Blade Pitch 75% span, deg	6
Airfoil	Clark-Y
Taper	None
Twist, deg	12 (Linear)
Solidity	0.090
Precone, deg	0
Tilt, deg	10

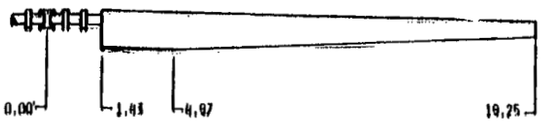

RADIUS m	CHORD, m
1.43	1.473
4.97	1.473
19.25	.457

Figure 1a - Mod-0 aluminum blade planform

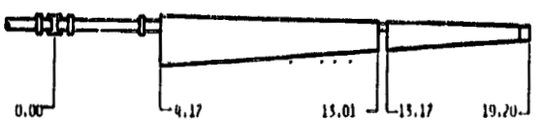

RADIUS, m	CHORD, m
4.17	1.964
13.01	1.171
13.17	1.154
19.20	.672

Figure 1b - Mod-0 steel spar blade planform

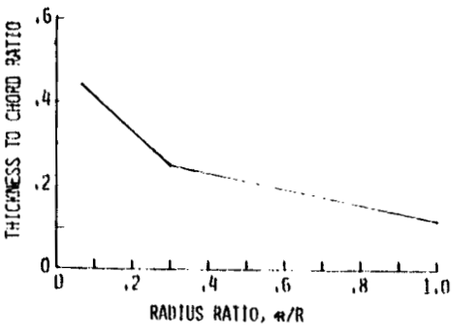

Figure 2a - Mod-0 aluminum blade thickness to chord ratio distribution

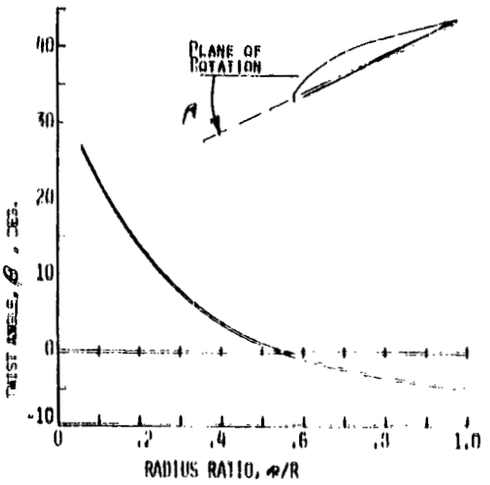

Figure 2b - Mod-0 aluminum blade twist distribution

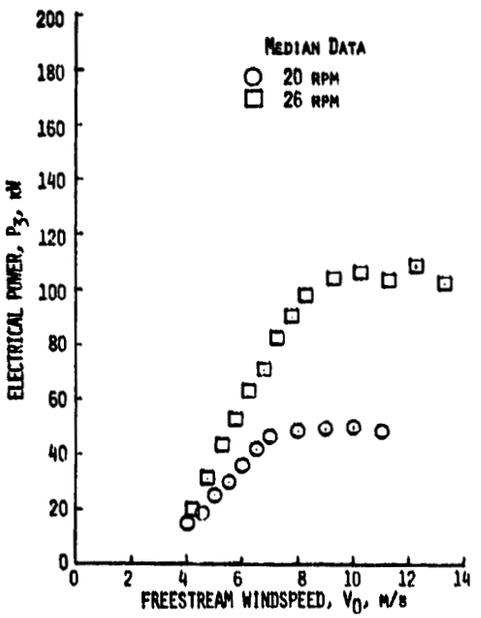

Figure 3 - Measured Performance of the Mod-0 aluminum blades at 20 and 26 rpm

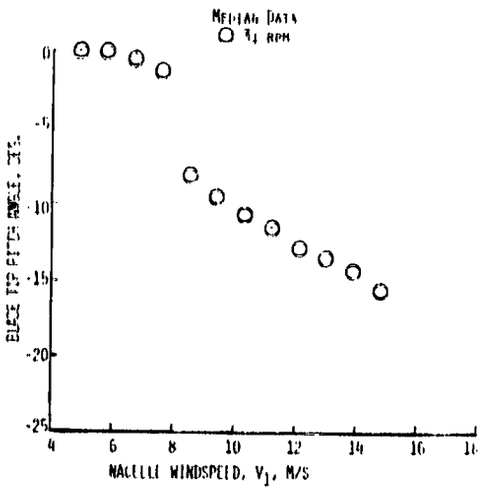

Figure 4 - Measured tip pitch angle versus windspeed for the Mod-0 steel spar, tip control blades

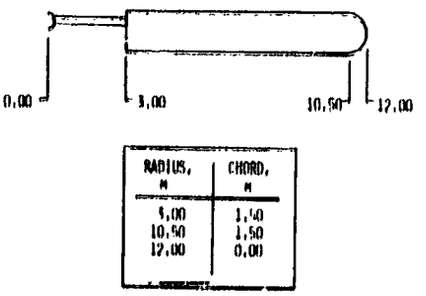

RADIUS, M	CHORD, M
3.00	1.40
10.50	1.50
12.00	0.00

Figure 6 - Danish Gedser wind turbine blade planform

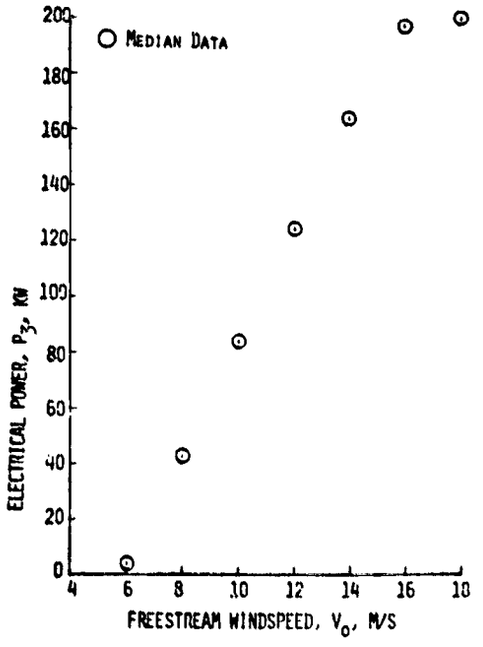

Figure 5 - Measured performance of the Danish Gedser wind turbine

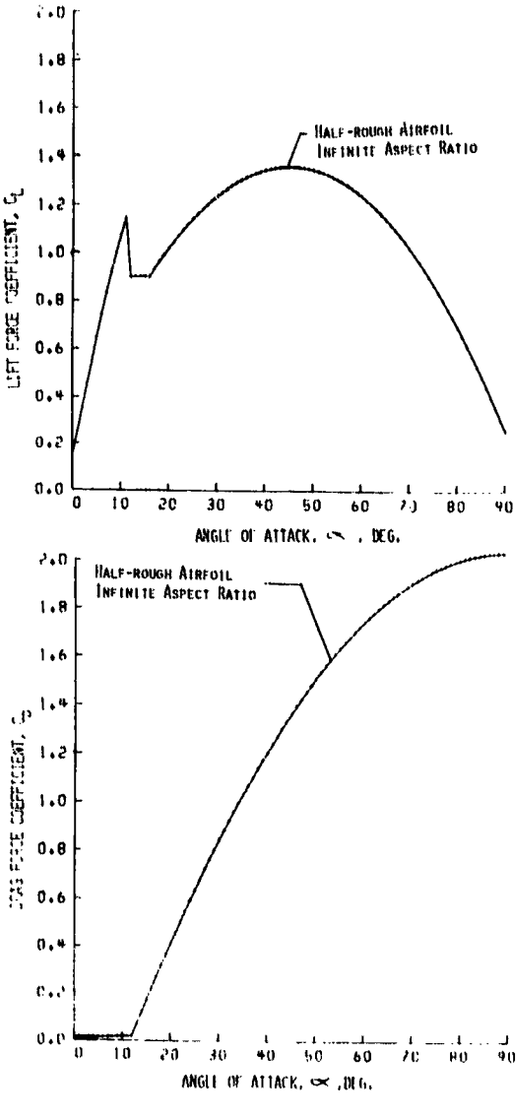

Figure 7 - Aerodynamic data for "half-rough" NACA 23018 airfoil

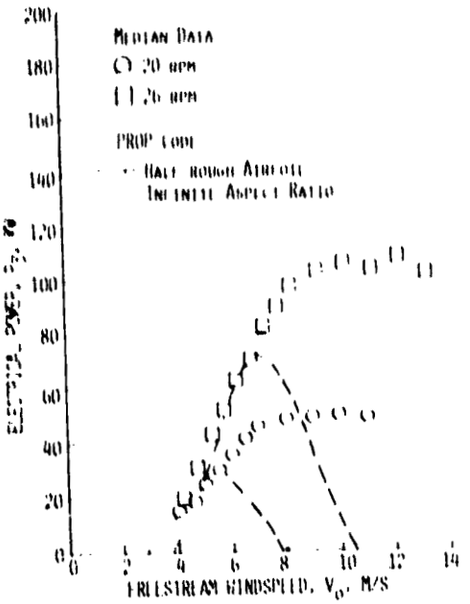

Figure 8 - Comparison of measured and calculated performance using classical theory for the Mod-0 aluminum blades

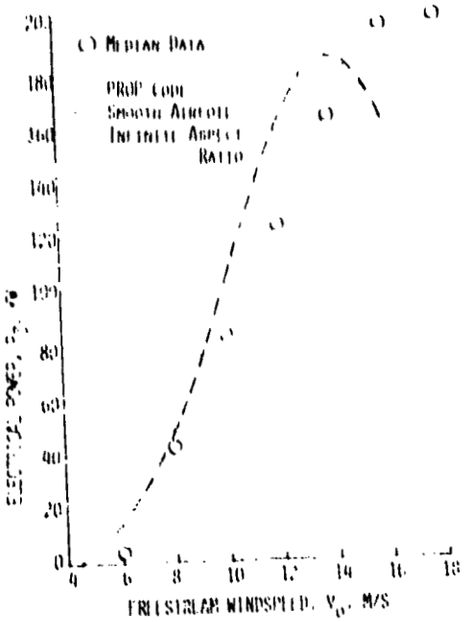

Figure 10 - Comparison of measured and calculated performance using classical theory for the Danish Gedser wind turbine

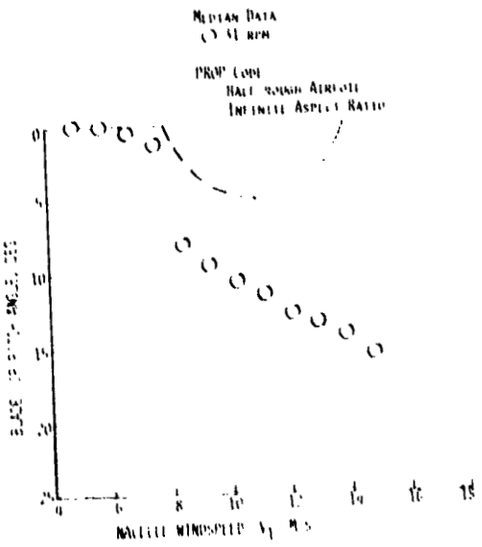

Figure 9 - Comparison of measured and calculated tip angle versus windspeed using classical theory for the Mod-0 steel spar, tip control blades

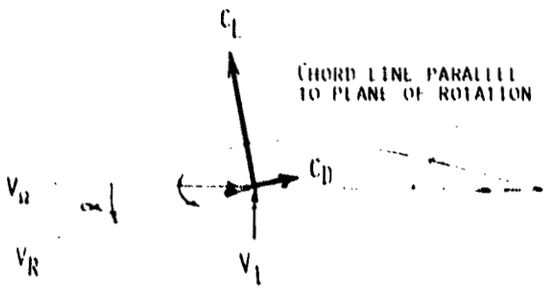

Figure 11 - Blade element wind velocity and force vector diagram

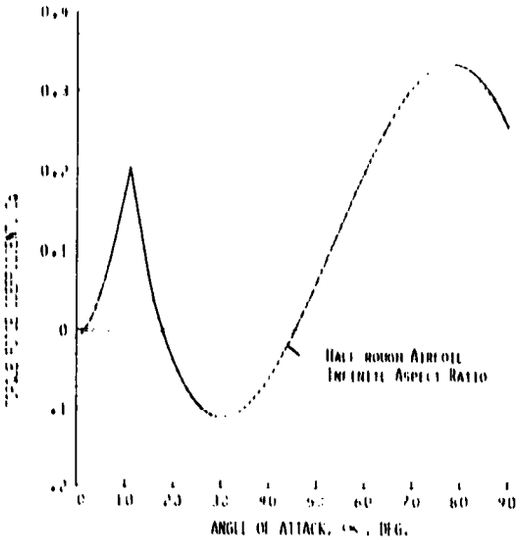

Figure 12 - Aerodynamic torque force coefficient versus angle of attack for "half-rough" NACA 23018 airfoil

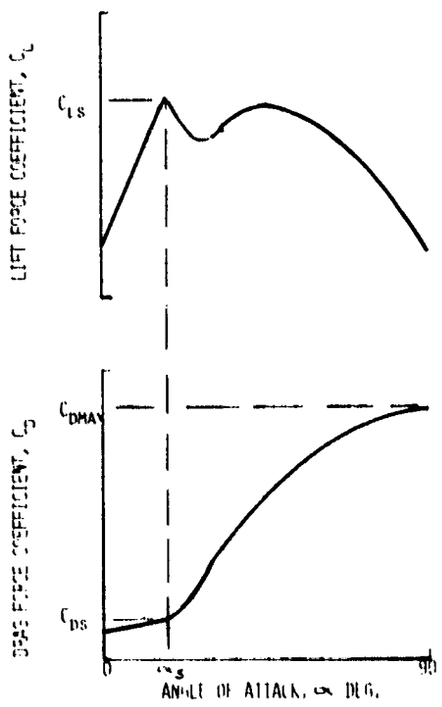

Figure 13 - General aerodynamic characteristics for idealized stall model

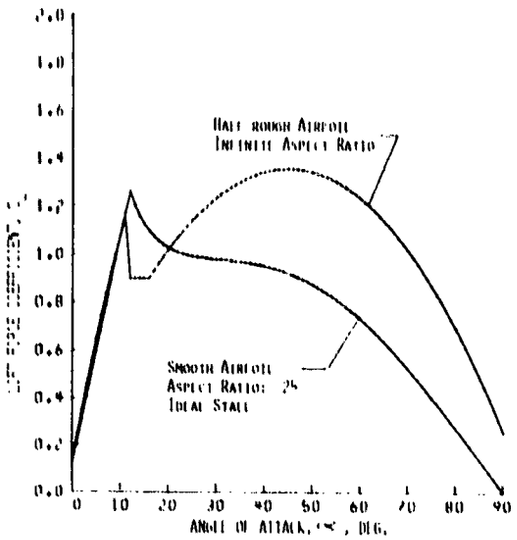

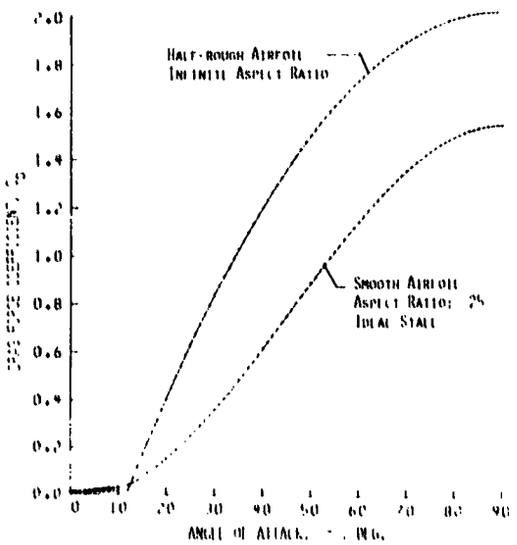

Figure 14 - Comparison of two dimensional "half-rough" and improved aerodynamic data

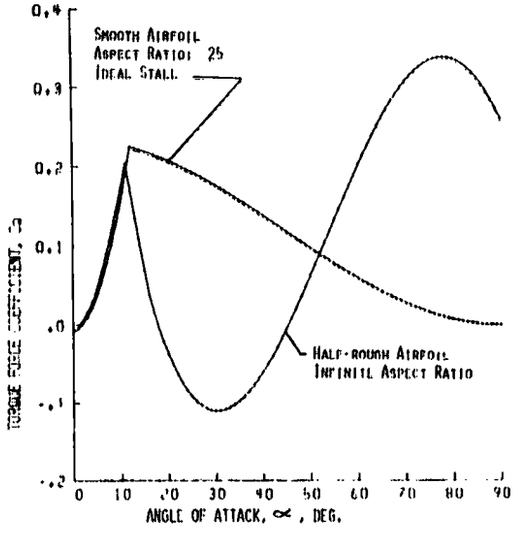

Figure 15 - Comparison of two dimensional "half-rough" and improved aerodynamic torque force coefficient

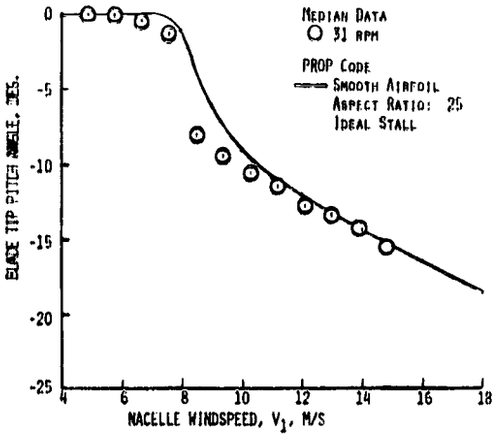

Figure 17 - Comparison of measured and calculated tip angle versus windspeed using improved aerodynamic data for the Mod-0 steel spar blades

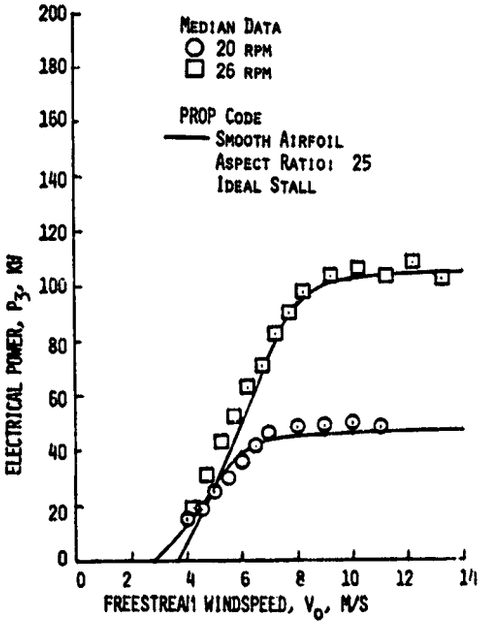

Figure 16 - Comparison of measured and calculated performance using improved aerodynamic data for the Mod-0 aluminum blades

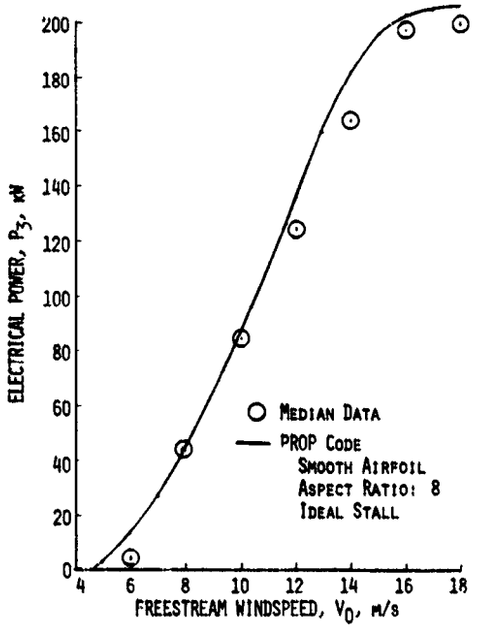

Figure 18 - Comparison of measured and calculated performance using improved aerodynamics for the Danish Gedser wind turbines

QUESTIONS AND ANSWERS

L. Viterna

From: B. Dahlroth

Q: Comment on the effect of dynamic stall.

A: *We did not observe any significant effects of dynamic stall even though the 230XX series airfoil were used on the MOD-0. System dynamic loads were well behaved during these tests.*

From: J. Dugundji

Q: How did you keep the turbine at constant RPM throughout the wind speed range? How do you keep it from overspeeding?

A: *The electrical generator is held at a near synchronous speed with respect to the electrical line. The actual rotor speed deviates from the nominal RPM due to slip i.. the fluid coupling in the drive train. A high speed shaft brake was available to prevent overspeed in an emergency upon loss of electrical load.*

From: Anonymous

Q: If the peak power is more than doubled by going from 20-26 RPM, what is the power limit from increasing RPM?

A: *There is no practical aerodynamic limit to maximum power with increasing RPM. At higher rotor speeds the rotor stalls at a higher windspeed and thus a much higher power.*

From: M. Rolland

Q: How would you characterize the starting ability of the fixed pitch rotor? Is there a sacrifice with fixed pitch?

A: *This is not addressed in the presentation. We have studied starting characteristics of fixed pitch rotors and believe it is possible to design a fixed pitch machine which will start in low winds and not be penalized significantly in performance. The zero twist blades on MOD-0 start with about 4 degrees of pitch in a 5 m/s wind. The 34 degree twisted blades start with 0 degrees of pitch in a similar wind.*

From: K. Foreman

Q: How do you explain the revised aero-characteristics of the blade after stall, also Reynolds number effects?

A: *We believe this is due to three-dimensional flow effects which are not accounted for using the classical blade element-momentum theory. The airfoil data is modeled at the Reynolds number at the 75 percent span of the blade.*

From: G. R. Kotley

Q: Do you have any experience of the effect on the stalled power curve of the smooth surface-laminar flow aerofoils, instead of the half-rough 23XXX series?

A: *Performance data for a NACA 645-618 airfoil is being reduced. Some results are given in John Glasgow's paper, "Stall-Induced Instability of a Teetered Rotor."*